

Production of Θ^+ in $\gamma + D \rightarrow \Lambda + \Theta^+$ and $\gamma + D \rightarrow \Sigma + \Theta^+$ reactions

V. Guzey

*Institut für Theoretische Physik II,
Ruhr-Universität Bochum, D-44780 Bochum, Germany*

Abstract

The $\gamma + D \rightarrow \Lambda + \Theta^+$ and $\gamma + D \rightarrow \Sigma + \Theta^+$ reactions can be used to determine the width of Θ^+ almost model-independently. We calculate the differential cross sections of the $\gamma + D \rightarrow \Lambda + \Theta^+$, $\gamma + D \rightarrow \Sigma + \Theta^+$ and relevant background reactions in the photon energy range $1.2 \leq E_\gamma \leq 2.6$ GeV. We determine the most favorable kinematic conditions and observables for the experimental studies of Θ^+ in the considered processes. We argue that a comparison of the $\gamma + D \rightarrow \Lambda + \Theta^+$ and $\gamma + D \rightarrow \Sigma + \Theta^+$ cross sections should unambiguously determine isospin of Θ^+ .

PACS numbers: 13.60.Rj, 14.20.Jn, 25.20.Lj

I. INTRODUCTION

Evidence for the existence of the pentaquark state Θ^+ [1] is now rather overwhelming. The initial experimental reports about the discovery of Θ^+ [2, 3, 4, 5, 6, 7, 8, 9, 10, 11, 12] will be followed by a series of dedicated high precision experiments aiming to study such properties of the new baryon as parity, spin and isospin. Hence, it is topical to analyze in which reactions and at which kinematic conditions production of Θ^+ is sufficiently copious and can be reliably estimated by hadronic phenomenology.

An important role in the present and future experimental investigations concerning Θ^+ is played by photoproduction on deuterium. In some cases, the deuterium target serves as a mere source of the proton and neutron targets and rescattering on the spectator nucleon simply enhances the Θ^+ signal [4]. In other cases, rescattering on the spectator nucleon is the source of Θ^+ production [12]. In this paper, we concern ourselves with the latter class of reactions. In particular, we consider the strangeness tagging $\gamma + D \rightarrow \Lambda(\Sigma) + \Theta^+$ reaction, where the interaction of the photon with one of the nucleons produces a hyperon (Λ or Σ) and a kaon. One then can choose kinematics where the produced kaon has the correct momentum to produce Θ^+ via the interaction with the other nucleon of the deuteron. The main advantage of the reaction is that the theoretical analysis is only weakly model-dependent: the differential cross section for the $\gamma + p \rightarrow \Lambda(\Sigma) + K^+$ has been measured and the $\gamma + p \rightarrow \Lambda(\Sigma) + K^+$ and $\gamma + n \rightarrow \Lambda(\Sigma) + K^0$ amplitudes have been phenomenologically parametrized; the deuteron wave function is known very well for the momentum range involved in the process; the dynamical information about Θ^+ enters only through the total width of Θ^+ , which can be treated as a free parameter and then determined by the comparison to experiment. However, since production of Θ^+ takes place through rescattering on the spectator nucleon of deuterium (see Fig. 1), the resulting cross section is suppressed by the nuclear wave function at high momenta (this suppression is under control).

II. $\gamma + D \rightarrow \Lambda(\Sigma) + \Theta^+$ CROSS SECTIONS

The reaction $\gamma + D \rightarrow \Lambda(\Sigma) + \Theta^+$ is described by two Feynman graphs presented in Fig. 1. We neglected the unknown final-state interactions between $\Lambda(\Sigma)$ and Θ^+ . It is important to note that the resulting scattering amplitude on deuterium crucially depends on interfer-

ence between the $\gamma p \rightarrow \Lambda(\Sigma) K^+$ and $\gamma n \rightarrow \Lambda(\Sigma) K^0$ (elementary) scattering amplitudes. This introduces certain model-dependence into our calculations since our results become dependent on the $\gamma n \rightarrow \Lambda(\Sigma) K^0$ amplitude, for which there is only a phenomenological parameterization and not experimental data.

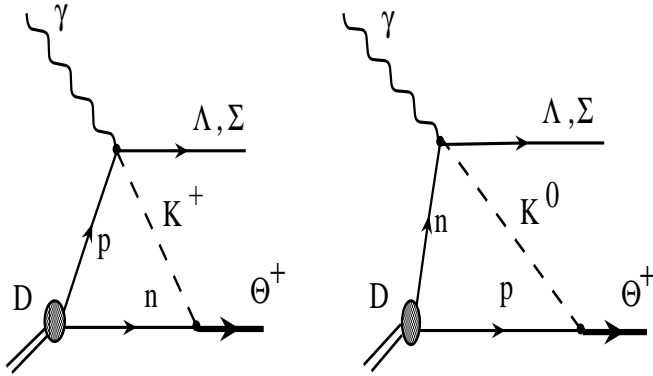


FIG. 1: Two graphs of $\gamma + D \rightarrow \Lambda(\Sigma) + \Theta^+$.

Our numerical analysis of the Feynman graphs in Fig. 1 showed that the scattering amplitude is predominantly imaginary in the considered kinematics. The imaginary part is found as a sum of all possible cuts of the diagrams in Fig. 1. It is clear that there are three possible cuts. However, cutting simultaneously the spectator nucleon (neutron in the left graph and proton in the right graph) and kaon lines gives the dominant contribution. This cut places the spectator nucleon and the kaon on mass shell.

After this cut, in the $\Theta^+ \rightarrow NK$ vertex all particles are on mass shell. This means that the corresponding expression is a function of the particle masses and the total width of Θ^+ and, hence, it does not depend on the spectator momentum.

The interacting nucleon (proton in left graph and neutron in the right graph of Fig. 1) is off mass shell. An examination of its energy denominator shows that the interacting nucleon is not far from its mass shell and, hence, to a good approximation can be treated as being on mass shell. Then, with a good accuracy, the $\gamma + N \rightarrow \Lambda + K$ amplitude in Fig. 1 depends only on the external four-momentum transfer $t = (p_\gamma - p_\Lambda)^2$ and the photon energy E_γ .

Details of the derivation of the scattering amplitude and cross sections corresponding to

Feynman graphs of Fig. 1 are given in Appendix A. Here we give the final expression for the differential cross section for the $\gamma + D \rightarrow \Lambda(\Sigma) + \Theta^+$ process

$$\frac{d\sigma^{\gamma+D \rightarrow \Lambda(\Sigma)+\Theta^+}}{dt} = 2\pi\Gamma^{tot} \frac{M_\Theta^3}{\sqrt{(M_\Theta^2 - m^2 - m_K^2)^2 - 4m^2m_K^2}} \frac{d\sigma^{p+n}}{dt} S(t), \quad (1)$$

where Γ^{tot} is the total width of Θ^+ and $M_\Theta = 1.540$ GeV is its mass; m is the nucleon mass and m_K is the kaon mass.

The factorized form of Eq. (1) is a consequence of the on-mass-shellness of all particles in the loop in Fig. 1. The first factor involving the masses and Γ^{tot} comes from the $\Theta^+ \rightarrow NK$ vertex.

We assumed that Θ^+ has spin 1/2 and isospin 0. Other spin and isospin assignments are considered in the end of this Section.

The second factor $d\sigma^{p+n}/dt$ is the differential cross section, which includes the $\gamma + p \rightarrow \Lambda(\Sigma) + K^+$ and $\gamma + n \rightarrow \Lambda(\Sigma) + K^0$ amplitudes and their interference. The differential cross section $d\sigma^{p+n}/dt$ at the photon beam energies 1.2 and 2 GeV is presented in Fig. 2 (solid curves). For comparison, we also give the $\gamma + p \rightarrow \Lambda(\Sigma) + K^+$ differential cross section (dashed curves).

Note that the momentum transfer squared from γ to Λ is defined as $t = (p_\gamma - p_\Lambda)^2$. This means that in Fig. 2, the minimal t (maximal $|t|$) corresponds to the forward scattering kaon in the center of mass frame.

Note also the important role of interference between the $\gamma + p \rightarrow \Lambda(\Sigma) + K^+$ and $\gamma + n \rightarrow \Lambda(\Sigma) + K^0$ amplitudes. At small values of t , which is the most interesting region for us, $d\sigma^{p+n}/dt$ is significantly larger than $d\sigma^p/dt$. Thus, the contribution of $\gamma + n \rightarrow \Lambda(\Sigma) + K^0$ significantly enhances the resulting $\gamma + D \rightarrow \Lambda(\Sigma) + \Theta^+$ cross section. The curves in Fig. 2 were obtained using the MAID data base and generator [13] consistent with the SAPHIR $\gamma + p \rightarrow \Lambda + K^+$ data [14, 16] and $\gamma + p \rightarrow \Sigma + K^+$ data [15, 16]. Note that the choice of the photon energy $E_\gamma = 1.2$ and 2 GeV is motivated by the constraints of the MAID generator, $0.9 < E_\gamma < 2.1$ GeV. Note also that the cross section for production of Σ is approximately two times larger than that of Λ .

It is important to note that since we took Θ^+ with isospin-0 for this calculation, the $\gamma + p \rightarrow \Lambda(\Sigma) + K^+$ and $\gamma + n \rightarrow \Lambda(\Sigma) + K^0$ amplitudes as generated by MAID enter with a relative plus sign.

The last factor in Eq. (1) describes the t -dependent suppression by the deuteron wave

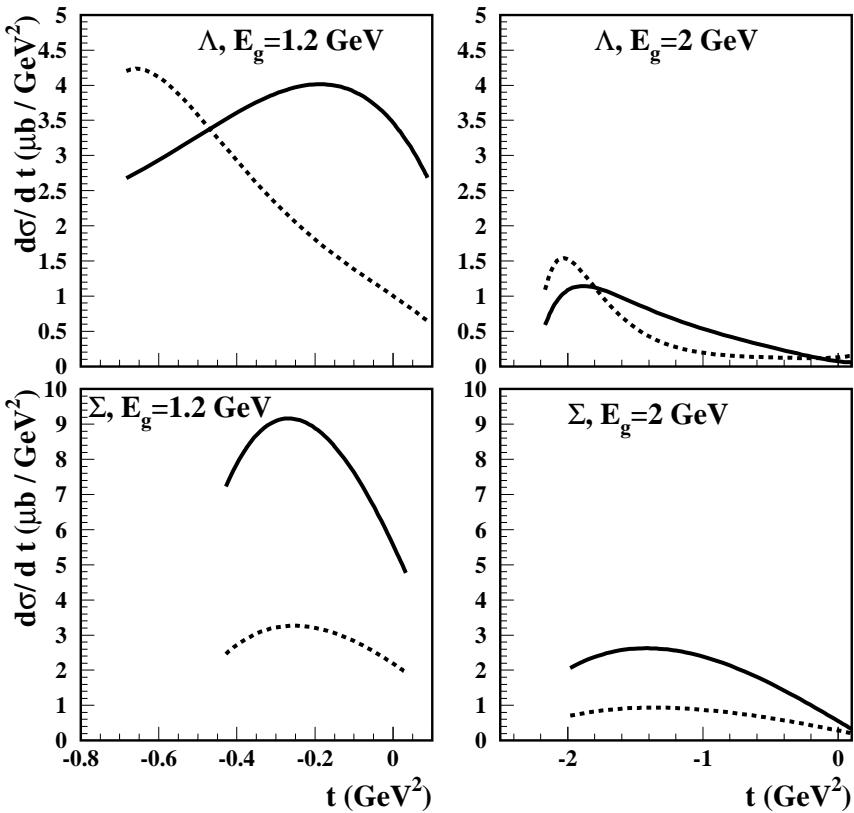


FIG. 2: The differential cross section $d\sigma^{p+n}/dt$, which includes both $\gamma + p \rightarrow \Lambda(\Sigma) + K^+$ and $\gamma + n \rightarrow \Lambda(\Sigma) + K^0$ amplitudes and their interference, as a function of the momentum transfer squared t from γ to Λ (solid curves). The $\gamma + p \rightarrow \Lambda(\Sigma) + K^+$ cross section $d\sigma^p/dt$ is given by the dashed curves. The upper panels correspond to Λ production, the lower panels correspond to Σ production.

function due to rescattering on the spectator nucleon (see Appendix A for details). We used the deuteron wave function with the Paris nucleon-nucleon potential [17]. Figure 3 shows $S(t)$ as a function of t . Note that within our approach, $S(t)$ does not depend on energy. Also, since masses of Λ and Σ are rather close, the nuclear factor $S(t)$ is the same for Λ and Σ production.

A very strong t -dependence of $S(t)$ suggests that the region $-0.2 < t < 0$ GeV 2 is most favorable for the experimental studies of the $\gamma + D \rightarrow \Lambda(\Sigma) + \Theta^+$ reaction.

The main results of the present paper, the differential cross sections for the $\gamma + D \rightarrow \Lambda + \Theta^+$

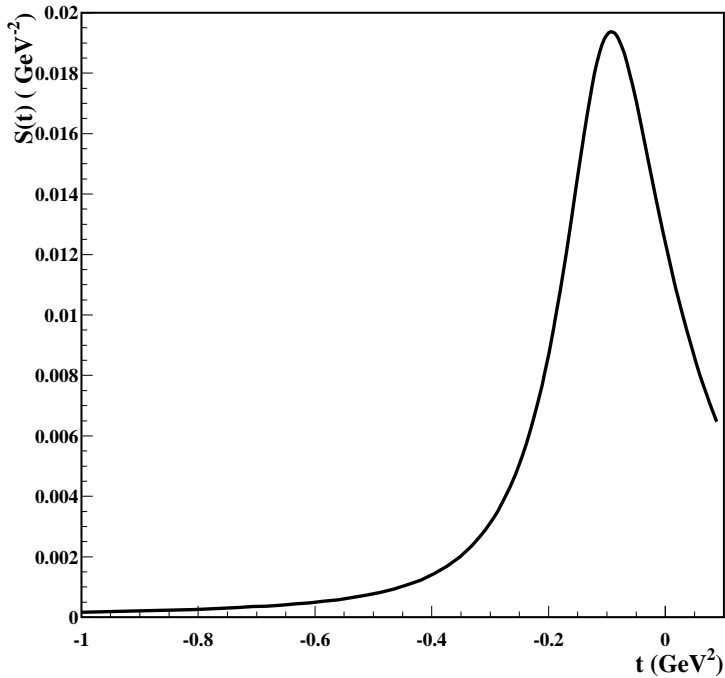


FIG. 3: The nuclear suppression factor $S(t)$.

and $\gamma + D \rightarrow \Sigma + \Theta^+$ processes, are presented in Figs. 4 and 5.

The differential cross section is calculated at four different photon energies, $E_\gamma = 1.2, 1.6, 2$ and 2.6 GeV, which correspond to the kinematics of SPring-8, JLab, SAPHIR and GRAAL experiments (the photon energy $E_\gamma = 2.6$ GeV is the largest energy at which there are $\gamma + p \rightarrow \Lambda(\Sigma) + K^+$ data). One sees that the cross sections are largest for $-0.2 < t < 0$ GeV^2 : this is the most favorable region of t for copious Θ^+ production. In this calculation we assumed that $\Gamma^{tot} = 5$ MeV. As follows from Eq. (1), the discussed cross sections depend linearly on Γ^{tot} . Therefore, if one wishes to use a different width of Θ^+ , $\bar{\Gamma}^{tot}$, the cross section of Θ^+ production should be rescaled by the factor $\bar{\Gamma}^{tot}/\Gamma^{tot}$.

One should note that at the moment the total width of Θ^+ is rather uncertain. Theoretical predictions for its values range from less than 15 MeV [1] to several MeV [18, 19]. The experimental determination of the width of Θ^+ is limited by the experimental resolution. The most stringent constraint is given by the DIANA collaboration [3], $\Gamma^{tot} < 9$ MeV. Only two experiments, HERMES [8] and ZEUS [11], appear to indicate a finite width of Θ^+ which is somewhat larger than the experimental resolution.

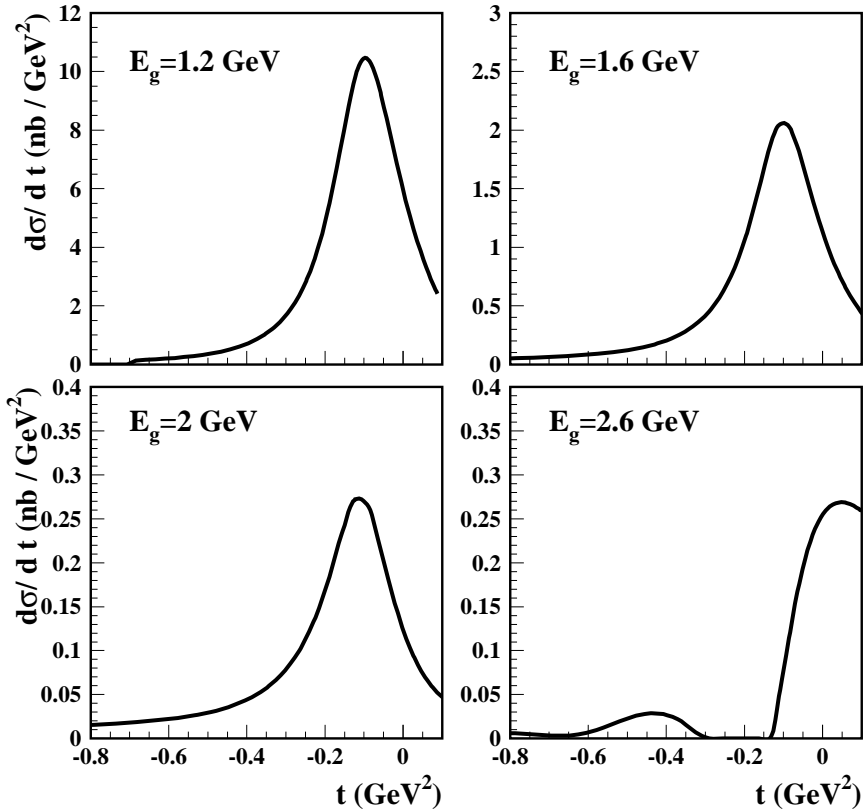


FIG. 4: The $\gamma + D \rightarrow \Lambda + \Theta^+$ differential cross section as a function of the momentum transfer t at different photon energies, $E_\gamma = 1.2, 1.6, 2$ and 2.6 GeV. The total width of Θ^+ is assumed $\Gamma^{tot} = 5$ MeV. In order to use a different width of Θ^+ , $\bar{\Gamma}^{tot}$, the curves in this figure should be scaled by the factor $\bar{\Gamma}^{tot}/\Gamma^{tot}$.

The $\gamma + D \rightarrow \Lambda(\Sigma) + \Theta^+$ cross section decreases rather rapidly with increasing photon energy. This is determined by the decrease of the $\gamma + p \rightarrow \Lambda(\Sigma) + K^+$ cross section [16] and, more importantly, by the changing t -dependence of the $\gamma + p \rightarrow \Lambda(\Sigma) + K^+$ and $\gamma + n \rightarrow \Lambda(\Sigma) + K^0$ differential cross sections. As the photon energy increases, the cross sections are peaked progressively at smaller c.m. scattering angles of the kaon, which translates to intermediate values of t in our kinematics, where the suppression due to the nuclear factor $S(t)$ is rather significant.

One sees from Figs. 4 and 5 that the photon energy $E_\gamma = 1.2$ GeV gives the largest Θ^+

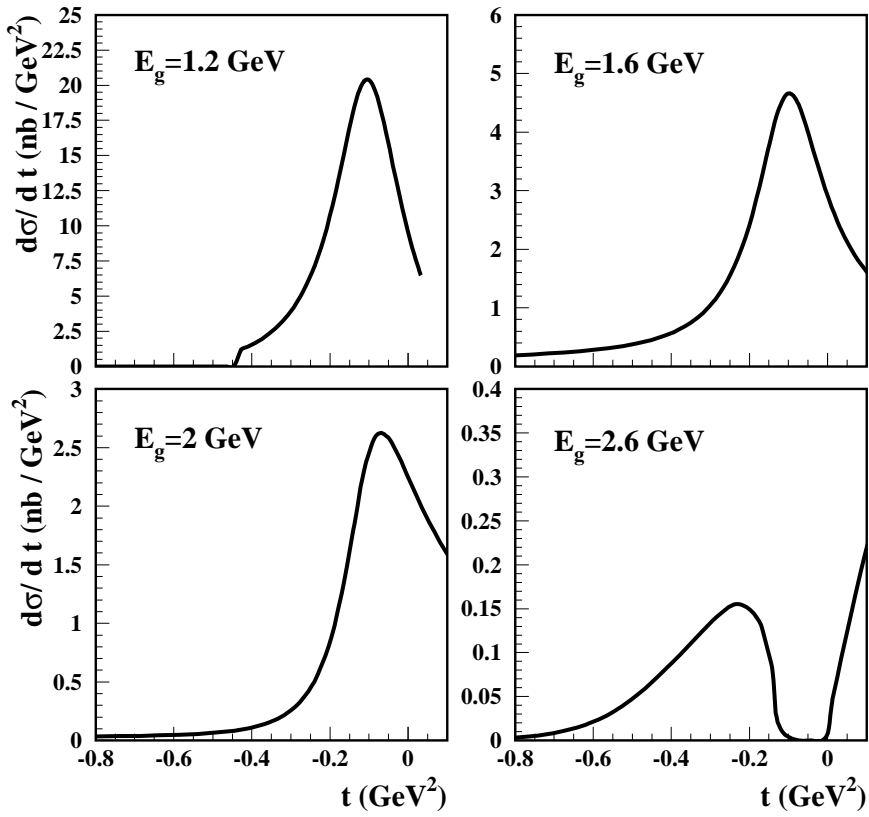


FIG. 5: The $\gamma + D \rightarrow \Sigma + \Theta^+$ differential cross section as a function of momentum transfer t at different photon energies, $E_\gamma = 1.2, 1.6, 2$ and 2.6 GeV. The total width of Θ^+ is assumed $\Gamma^{tot} = 5$ MeV. In order to use a different width of Θ^+ , $\bar{\Gamma}^{tot}$, the curves in this figure should be scaled by the factor $\bar{\Gamma}^{tot}/\Gamma^{tot}$.

production cross section (notice the y -axis scale change as we increase the photon energy).

While for $E_\gamma = 1.2, 1.6$ and 2 GeV we used the results of MAID [13], for $E_\gamma = 2.6$ GeV we directly used the recent SAPHIR experimental data for $\gamma + p \rightarrow \Lambda(\Sigma) + K^+$ [16]. Then we assumed that the $\gamma + p \rightarrow \Lambda(\Sigma) + K^+$ and $\gamma + n \rightarrow \Lambda(\Sigma) + K^0$ scattering amplitudes are equal. Therefore, our results at $E_\gamma = 2.6$ GeV bear the largest theoretical uncertainty and should be considered as a qualitative upper limit. This explains the shape of the curves at $E_\gamma = 2.6$ GeV: for instance, the presence of the dip at $t \approx -0.2$ GeV 2 in Fig. 4 originates from the almost zero $\gamma + p \rightarrow \Lambda + K^+$ cross section at $\cos(\Theta_{K^+}^{cms}) \approx -0.25$ [16].

Integrating the differential cross sections over t , we obtain the corresponding total cross

sections, which are summarized in Table 1.

E_γ , GeV	$\sigma^{\gamma+D \rightarrow \Lambda + \Theta^+}$, nbarn	$\sigma^{\gamma+D \rightarrow \Sigma + \Theta^+}$, nbarn
1.2	2.51	4.44
1.6	0.57	1.42
2	0.090	0.74
2.6	0.055	0.063

TABLE I: Integrated $\gamma + D \rightarrow \Lambda + \Theta^+$ and $\gamma + D \rightarrow \Sigma + \Theta^+$ cross sections at different photon energies E_γ . The total width of Θ^+ is assumed $\Gamma^{tot} = 5$ MeV.

One should note that in the considered processes, Λ can be produced either directly in the $\gamma + N \rightarrow \Lambda + K$ vertex or in the $\Sigma^0 \rightarrow \Lambda + \gamma$ decay. Hence, a special attention should be payed to distinguish these two ways of producing Λ in the experiment.

Also, one can consider other than spin-1/2 and isospin-0 assignments for Θ^+ . The issue of isospin of Θ^+ constitutes an interesting theoretical question, see for instance [20, 21]. If Θ^+ has spin-3/2, then the final expression for the differential cross section in Eq. (8) should be twice as large. This is a consequence of the fact that spin-3/2 Θ^+ has twice as many polarization states compared to the spin-1/2 Θ^+ .

If Θ^+ has isospin-1, this introduces a minus sign between the two Feynman graphs in Fig. 1. Indeed, in this case isospin invariance indicates that the $\Theta^+ p K^0$ and $\Theta^+ n K^+$ vertices have opposite signs (see Appendix B for details). As a result, the $\gamma + D \rightarrow \Lambda + \Theta^+$ cross section becomes enhanced, while the $\gamma + D \rightarrow \Sigma^0 + \Theta^+$ cross section is significantly reduced, as compared to the isospin-0 case. The corresponding Θ^+ isospin-1 differential cross sections at two photon energies, $E_\gamma = 1.2$ and 1.6 GeV, are presented in Fig. 6.

Figure 6 ($I_\Theta = 1$) should be compared to Figs. 5 and 8 ($I_\Theta = 0$). In the former case, the $\gamma + D \rightarrow \Lambda + \Theta^+$ cross section is enhanced by approximately factor of two as compared to the $I_\Theta = 0$ case. On the other hand, the $\gamma + D \rightarrow \Sigma^0 + \Theta^+$ cross section becomes reduced by approximately factor of ten as compared to the $I_\Theta = 0$ case. This result can be explained as follows. If isospin of Θ^+ is zero, the $\gamma + D \rightarrow \Lambda + \Theta^+$ reaction involves the $I = 0$ component of the initial photon, while $\gamma + D \rightarrow \Sigma + \Theta^+$ reaction involves the $I = 1$ component of the photon. An analogy with the vector meson dominance model suggests that the interaction mediated by the $I = 1$ component is stronger than by the $I = 0$ component, exactly as we

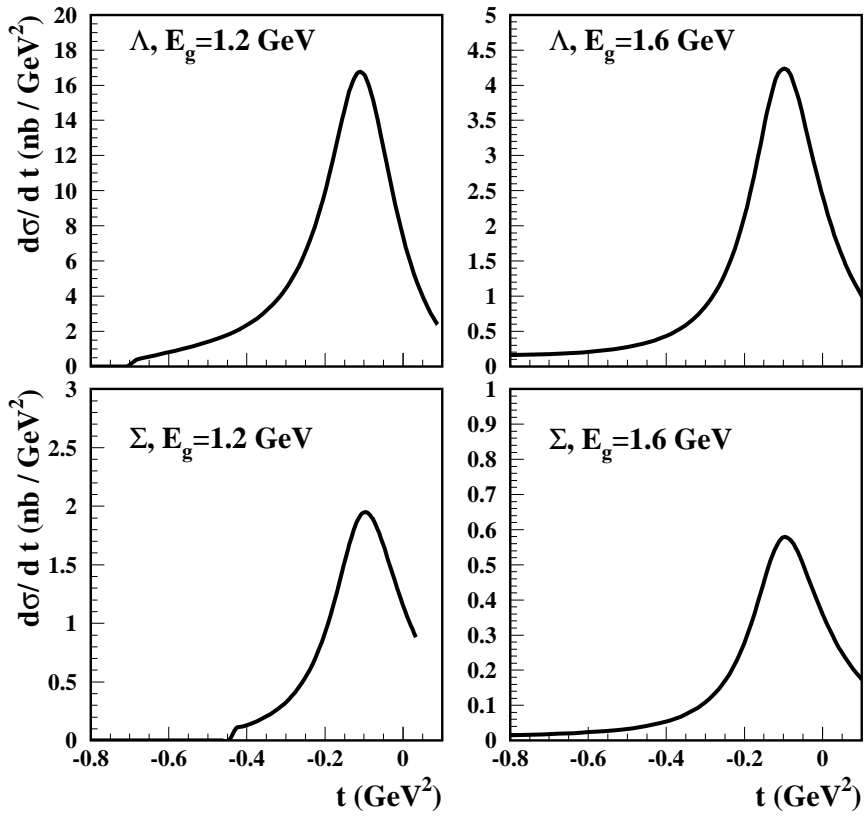


FIG. 6: Θ^+ with isospin-1. The $\gamma + D \rightarrow \Sigma + \Theta^+$ (upper panels) and $\gamma + D \rightarrow \Sigma^0 + \Theta^+$ (lower panels) differential cross sections as functions of the momentum transfer t at different photon energies, $E_\gamma = 1.2$ and 1.6 GeV. It is assumed that $\Gamma^{tot} = 5$ MeV.

observe. On the other hand, if isospin of Θ^+ is 1, the situation is just the opposite and production of Λ is expected to be larger than production of Σ .

A comparison of the $\gamma + D \rightarrow \Lambda + \Theta^+$ and $\gamma + D \rightarrow \Sigma^0 + \Theta^+$ rates can clearly distinguish between the Θ^+ with isospin-0 and isospin-1 scenarios. Indeed, while the absolute value of the cross sections is uncertain due to the uncertainty in the total width of Θ^+ as well as due to possible final state interactions. However, the ratio of the $\gamma + D \rightarrow \Lambda + \Theta^+$ and $\gamma + D \rightarrow \Sigma^0 + \Theta^+$ cross sections (let us denote it by R) is insensitive to Γ^{tot} which cancels in the ratio. In addition, the final state interaction is a correction and, hence, cannot change R too much. Since the ratio R changes from $R \approx 0.5$ at $t \approx -0.1 \text{ GeV}^2$ (if Θ^+ has isospin-0) to $R \approx 8$ (in the isospin-1 case), it should be possible to experimentally distinguish between

these two cases.

If one assumes that $I_\Theta = 1$, in addition to the $\Sigma^0\Theta^+$ final state, one can consider production of $\Sigma^+\Theta^0$ and $\Sigma^-\Theta^{++}$ states. It follows from isospin conservation that $\sigma(\gamma+D \rightarrow \Sigma^+\Theta^0) = \sigma(\gamma+D \rightarrow \Sigma^-\Theta^{++})$. However, based solely on isospin conservation, $\sigma(\gamma+D \rightarrow \Sigma^+ + \Theta^0)$ and $\sigma(\gamma+D \rightarrow \Sigma^- + \Theta^{++})$ cannot be related to $\sigma(\gamma+D \rightarrow \Sigma^0 + \Theta^+)$.

We also note that the Θ^+ production mechanism of Fig. 1 cannot produce Θ^+ with isospin-2.

III. BACKGROUND ESTIMATES, INTERFERENCE WITH SIGNAL

The main background reaction $\gamma+D \rightarrow \Lambda(\Sigma) + K^+ + n$ is presented in Fig. 7. Since the other background reaction $\gamma+D \rightarrow \Lambda(\Sigma) + K^0 + p$ involves the unmeasured $\gamma+n \rightarrow \Lambda(\Sigma) + K^0$ amplitude, we shall concentrate on the process in Fig. 7.

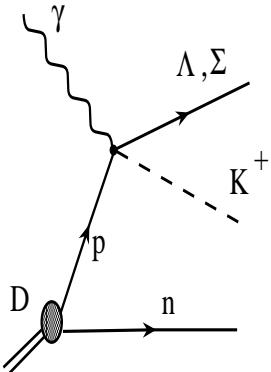


FIG. 7: The dominant background reaction.

The background process plays a two-fold role. First, a detailed examination shows that interference with the signal enhances Θ^+ production (see Appendix B for details). The differential interference cross section can be cast in the form of Eq. (1)

$$\frac{d\sigma^I}{dt} = 2\pi\Gamma^{tot} \frac{M_\Theta^3}{\sqrt{(M_\Theta^2 - m^2 - m_K^2)^2 - 4m^2m_K^2}} \frac{d\sigma_{\text{elem}}^I}{dt} S(t), \quad (2)$$

where σ_{elem}^I is the interference cross section obtained using the interference amplitude $|\mathcal{A}_{\text{elem}}^I|^2 = (\mathcal{A}^p + \mathcal{A}^n)(\mathcal{A}^p)^* + (\mathcal{A}^p + \mathcal{A}^n)^*\mathcal{A}^p$ involving the $\gamma + p \rightarrow \Lambda(\Sigma) + K^+$ (denoted as \mathcal{A}^p) and $\gamma + n \rightarrow \Lambda(\Sigma) + K^0$ (denoted as \mathcal{A}^n) amplitudes.

Hence, the signal plus interference cross section takes the following compact form

$$\frac{d\sigma^{\gamma+D \rightarrow \Lambda(\Sigma)+n+K^+}}{dt} = 2\pi\Gamma^{\text{tot}} \frac{M_\Theta^3}{\sqrt{(M_\Theta^2 - m^2 - m_K^2)^2 - 4m^2m_K^2}} \left(\frac{1}{2} \frac{d\sigma^{p+n}}{dt} + \frac{d\sigma_{\text{elem}}^I}{dt} \right) S(t), \quad (3)$$

where an additional factor 1/2 in front of the first term is a consequence of the 1/2-branching ratio of the $\Theta^+ \rightarrow nK^+$ decay. Note that the simple form of Eq. (3) holds only for the cross sections integrated over the final neutron momentum (see discussion below).

The second aspect of the background process is that it produces the same final state as the signal process but does not carry any information (unlike the interference term) about Θ^+ . Hence, we intend to find kinematic conditions where the signal plus interference cross section is larger than the purely background contribution. It is important to point out that in general, the purely background (Born) cross section of Fig. 7 is much larger than the rescattering cross section of Fig. 1. The relative magnitude of these cross sections is determined predominantly by the nuclear suppression factor. While the Born amplitude is proportional to $\psi_D(p_s)$ with p_s being the final nucleon (spectator) momentum, the rescattering amplitude involves $\int dk k \psi_D(k)$. Therefore, one way to suppressed the purely background cross section is to choose relatively large spectator (neutron in Fig. 7) momenta.

Thus, it is important to discuss how different contributions depend on p_s . The p_s -dependence of the signal cross section is rather weak and is determined by the neutron-kaon phase space. The interference term depends on p_s much stronger through $\psi_D(p_s)$. In addition, the interference term is suppressed by the smallness of the total width of Θ^+ and the loop integral involving the deuteron wave function. The p_s -dependence of the purely background contribution is the strongest: the cross section is proportional to $|\psi_D(p_s)|^2$. However, this suppression is still not sufficient for the reduction of the background to the signal level: One needs to impose an additional constraint on the neutron-kaon invariant mass, see Eq. (4).

The theoretical analysis of the Feynman diagram in Fig. 7 is rather straightforward and is detailed in Appendix B. Since we aim to estimate the level of background under the Θ^+ resonance peak in the K^+ -neutron system, we impose the condition that in Fig. 7, the

invariant mass of the K^+ -neutron system, $M_{K^+ n}$, belongs to the interval, for instance,

$$M_\Theta - 10 \text{ MeV} \leq M_{K^+ n} \leq M_\Theta + 10 \text{ MeV}. \quad (4)$$

The value of 10 MeV is chosen as a realistic example with only one constraint in mind that 10 MeV resolution is clearly within the reach of future dedicated experiments on Θ^+ production.

The purely background $\gamma + D \rightarrow \Lambda(\Sigma) + K^+ + n$ double differential cross sections corresponding to Fig. 7 at different values of the momentum of the spectator neutron are presented in Fig. 8 by dashed curves. They should be compared to solid curves, which represent the signal plus interference $\gamma + D \rightarrow \Lambda(\Sigma) + K^+ + n$ cross section (see Appendix B for the exact expressions). The interference cross section is given by the dot-dashed curves. Note that interference with the background increases the signal. All curves correspond to $E_\gamma = 1.2$ GeV, where Θ^+ production is largest.

As one can see from Fig. 8, choosing a sufficiently high spectator momentum, $p_s = 300$ and 400 MeV/c and above, significantly reduces the background without changing the position and shape of the resonance peak. Hence, detection of a spectator nucleon (neutron) in coincidence with $\Lambda(\Sigma)$ presents a good opportunity to increase the signal to background ratio under the Θ^+ peak in the Θ^+ photoproduction on deuterium.

If experimental resolution in the final neutron-kaon invariant mass is at the level of several MeV and luminosity is sufficiently high, one can also study the shape of the Θ^+ production cross section as a function of $M^2 = (p_n + p_K)^2$ and clearly separate the signal from the background. An example is presented in Fig. 9, where we plot the signal plus interference triple differential cross section (solid curves) and the purely background triple differential cross section (dashed curves) as functions of M^2 . The kinematics is maximally favorable for the signal extraction: $E_\gamma = 1.2$ GeV, $t = -0.1$ GeV 2 and $p_s = 300$ MeV/c. One can see in Fig. 9 that the distinctive Breit-Wigner curve of the signal plus interference (solid curves) dominates the flat background distribution (dashed curves).

IV. CONCLUSIONS AND DISCUSSION

Among a multitude of Θ^+ photoproduction mechanisms, we single out the $\gamma + D \rightarrow \Lambda(\Sigma) + \Theta^+$ process as being weakly model-dependent. The $\gamma + D \rightarrow \Lambda(\Sigma) + \Theta^+$ cross

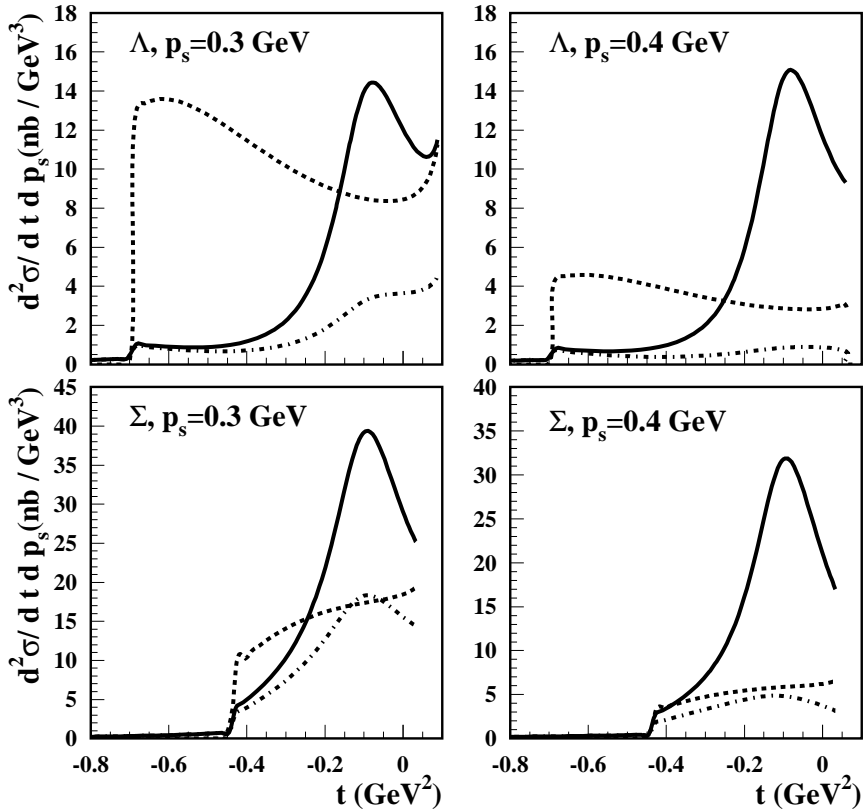


FIG. 8: The $\gamma + D \rightarrow \Lambda(\Sigma) + n + K^+$ double differential cross sections as functions of t at different spectator momenta p_s . The solid curves represent the signal plus interference cross section; the dash-dotted curves give the interference cross section; the dashed curves give the purely background cross section. The total width of Θ^+ is assumed $\Gamma^{tot} = 5$ MeV; the photon energy $E_\gamma = 1.2$ GeV.

section involves the measured $\gamma + p \rightarrow \Lambda(\Sigma) + K^+$ and phenomenologically parametrized $\gamma + n \rightarrow \Lambda(\Sigma) + K^0$ amplitudes, the well established deuteron wave function and the total width of Θ^+ . Therefore, the $\gamma + D \rightarrow \Lambda(\Sigma) + \Theta^+$ process is a very good candidate reaction for a precise measurement of the Θ^+ width.

We studied the $\gamma + D \rightarrow \Lambda(\Sigma) + \Theta^+$ differential cross section and found it to be sharply peaked for $-0.2 < t < 0$ GeV^2 , where $t = (p_\gamma - p_\Lambda)^2$. Hence, this kinematic region is most favorable for the experimental studies.

We performed our analysis of the $\gamma + D \rightarrow \Lambda(\Sigma) + \Theta^+$ cross section for a range of the photon energies, $1.2 \leq E_\gamma \leq 2.6$ GeV, which almost covers the energy range of SPring-8,

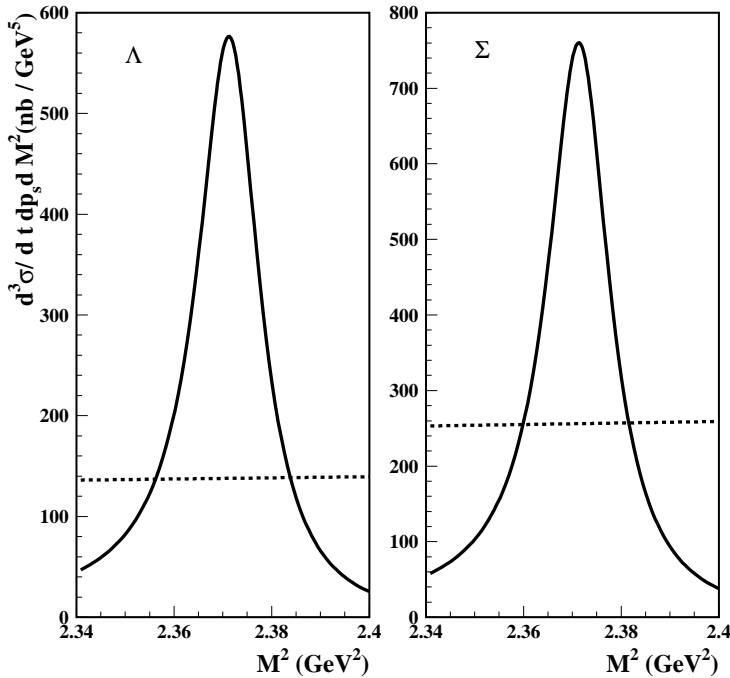


FIG. 9: The $\gamma + D \rightarrow \Lambda(\Sigma) + n + K^+$ triple differential cross sections as functions of the proton-kaon invariant mass squared at $E_\gamma = 1.2$ GeV, $t = -0.1$ GeV 2 and $p_s = 300$ MeV/c. The solid curves represent the signal plus interference cross section, the dashed curves give the purely background cross section.

TJNAF, SAPHIR and GRAAL experiments. It is found that $\gamma + D \rightarrow \Lambda(\Sigma) + \Theta^+$ cross section is largest at the smallest studied energy, $E_\gamma = 1.2$ GeV.

In order to understand if the extraction of Θ^+ from the $\gamma + D \rightarrow \Lambda(\Sigma) + \Theta^+$ data is possible, we estimated the rate of the background reaction $\gamma + D \rightarrow \Lambda(\Sigma) + K^+ + n$. We showed that the signal to background ratio is large when one chooses sufficiently large momenta of the spectator neutron, $p_s > 300$ MeV/c.

In addition, if experimental accuracy in the determination of the final neutron-kaon invariant mass is at the level of several MeV, one can also study the Θ^+ photoproduction cross section as a function of that invariant mass. The shape of the resulting distribution will clearly separate the signal from the background, see Fig. 9.

Our calculations in this paper are based on the assumption that Θ^+ has spin-1/2 and isospin-0. If Θ^+ is assigned spin-3/2, then the signal and interference cross sections are twice

as large. The relative rates of $\Lambda\Theta^+$ and $\Sigma\Theta^+$ production are very sensitive to isospin of Θ^+ . If Θ^+ has isospin-0, production of Σ is approximately twice as large as production of Λ . However, if we suppose that Θ^+ has isospin-1, production of Σ is significantly smaller than production of Λ .

Another important and yet undetermined characteristics of Θ^+ is its parity. Our prediction for the $\gamma + D \rightarrow \Lambda(\Sigma) + \Theta^+$ differential cross section does not depend on the Θ^+ parity since Θ^+ enters into our analysis only through its mass and total width. Overall, it appears that the $\gamma + D \rightarrow \Lambda(\Sigma) + \Theta^+$ reaction does not seem to be a good candidate to study parity of Θ^+ . In general, the $\gamma + D \rightarrow \Lambda(\Sigma) + \Theta^+$ amplitude can be parametrized in terms of twelve functions. Since the number of unknown functions is rather large, choosing different polarizations of the photon, deuteron and $\Lambda(\Sigma)$ is not sufficient to produce unambiguous and model-independent relations between polarization observables and parity of Θ^+ , as was suggested for the $\gamma + N \rightarrow \bar{K} + \Theta^+$ reaction [22].

Acknowledgments

It is a pleasure to thank Mark Strikman and Maxim Polyakov for continuing interest and illuminating discussions concerning the $\gamma + D \rightarrow \Lambda(\Sigma) + \Theta^+$ reactions. We also thank Kazuo Tsuchima for the discussion of initial drafts of the present paper, as well as K. Goeke and V. Metag. This work is supported by the Sofia Kovalevskaya Program of the Alexander von Humboldt Foundation.

Appendix A

In this appendix, we derive the master equation for the $\gamma + D \rightarrow \Lambda(\Sigma) + \Theta^+$ cross section, Eq. (1). The scattering amplitude corresponding to either one of the Feynman graphs of Fig. 1 reads

$$\mathcal{A} = i \int \frac{d^4 k}{(2\pi)^4} \bar{u}(p_\Theta) \hat{\Gamma}_\Theta \frac{\hat{k} + m}{k^2 - m^2 + i0} \frac{1}{(p_\Theta - k)^2 - m_K^2 + i0} \bar{u}(p_\Lambda) \hat{\Gamma}_\Lambda \frac{\hat{p}_D - \hat{k} + m}{(p_D - k)^2 - m^2 + i0} \hat{\Gamma}_D, \quad (5)$$

where k is the momentum of the spectator nucleon; the $\hat{\Gamma}_\Theta$ vertex describes the $\Theta^+ \rightarrow NK$ transition; the $\hat{\Gamma}_\Lambda$ vertex describes the $\gamma + N \rightarrow \Lambda(\Sigma) + K$ transition; $\hat{\Gamma}_D$ describes the $D \rightarrow NN$ transition. For brevity, all spin polarization indices are implicit.

An explicit calculations shows that the imaginary part dominates the scattering amplitude in Eq. (5). The imaginary part is found by taking all possible cuts of the graphs in Fig. 1. Cutting through the spectator nucleon and the kaon gives the principal contribution and the resulting amplitude reads

$$\begin{aligned} Im\mathcal{A} = & \frac{1}{16\pi} \int \frac{dkk}{E} \frac{\Theta(E_\Theta - E)}{p_\Theta} \Theta \left(-1 < \frac{E_\Theta E - a}{p_\Theta k} < 1 \right) \bar{u}(p_\Theta) \hat{\Gamma}_\Theta u(k) \\ & \times \bar{u}(p_\Lambda) \hat{\Gamma}_\Lambda u(p_D - k) \frac{1}{(p_D - k)^2 - m^2 + i0} \bar{u}(k) \bar{u}(p_D - k) \hat{\Gamma}_D, \end{aligned} \quad (6)$$

where E_Θ and p_Θ is the energy and momentum of Θ^+ in the deuteron rest frame; $a = (M_\Theta^2 + m^2 - m_K^2)/2$.

In the $\Theta^+ \rightarrow NK$ vertex all particles are on mass shell. Therefore, $\bar{u}(p_\Theta) \hat{\Gamma}_\Theta u(k)$ does not depend on the momentum k and can be expressed solely through the masses of Θ^+ , kaon and nucleon and the total width of Θ^+ .

The $D \rightarrow NN$ vertex $\hat{\Gamma}_D$ is expressed through the non-relativistic deuteron wave function ψ_D

$$\frac{1}{(p_D - k)^2 - m^2 + i0} \bar{u}(k) \bar{u}(p_D - k) \hat{\Gamma}_D = \sqrt{(2\pi)^3 2m} \psi_D(k) \quad (7)$$

where the deuteron polarization is implicit.

Finally, since the nuclear wave function has a very strong dependence on the momentum k , the elementary amplitude $\bar{u}(p_\Lambda) \hat{\Gamma}_\Lambda u(p_D - k)$ can be taken out of integration at some average momentum $\langle k \rangle$. It is important to emphasize that the resulting amplitude is a sum of both graphs in Fig. 1 such that it involves the coherent sum of the amplitudes $\gamma + p \rightarrow \Lambda(\Sigma^0)K^+$ and $\gamma + n \rightarrow \Lambda(\Sigma^0)K^0$.

The resulting spin-averaged differential cross section takes the following factorized form

$$\frac{d\sigma^{\gamma+D \rightarrow \Lambda(\Sigma)+\Theta^+}}{dt} = 2\pi \Gamma^{tot} \frac{M_\Theta^3}{\sqrt{(M_\Theta^2 - m^2 - m_K^2)^2 - 4m^2 m_K^2}} \frac{d\sigma^{p+n}}{dt} S(t), \quad (8)$$

where Γ^{tot} is the total width of Θ^+ .

This derivation assumed that Θ^+ has spin-1/2. If we assumed that it has spin-3/2, the final expression for the differential cross section in Eq. (8) would be twice as large. This is a consequence of the fact that spin-3/2 Θ^+ has twice as many polarization states compared to the spin-1/2 Θ^+ .

The differential cross section $d\sigma^{p+n}/dt$ involves the sum of the $\gamma + p \rightarrow \Lambda(\Sigma^0)K^+$ ampli-

tude (denoted \mathcal{A}^p) and the $\gamma + n \rightarrow \Lambda(\Sigma^0)K^0$ amplitude (denoted \mathcal{A}^n)

$$\frac{d\sigma^{p+n}}{dt} = \frac{1}{64\pi(E_\gamma m)^2} |\mathcal{A}^p + \mathcal{A}^n|^2. \quad (9)$$

Both amplitudes are taken as generated by the MAID generator [13] except for the case $E_\gamma = 2.6$ GeV, when we assumed that $\mathcal{A}^p = \mathcal{A}^n$ and took $|\mathcal{A}^p|^2$ from the experimental data [16].

Note that if Θ^+ has isospin-0, the $\gamma + p \rightarrow \Lambda(\Sigma^0)K^+$ and $\gamma + n \rightarrow \Lambda(\Sigma^0)K^0$ amplitudes should be added. However, if Θ^+ has isospin-1, the $\gamma + p \rightarrow \Lambda(\Sigma^0)K^+$ and $\gamma + n \rightarrow \Lambda(\Sigma^0)K^0$ amplitudes should be subtracted, which leads to an enhancement of the $\gamma + D \rightarrow \Lambda + \Theta^+$ cross section and a significant suppression of the $\gamma + D \rightarrow \Sigma^0 + \Theta^+$ cross section (see Fig. 6).

The factor $S(t)$ describes the suppression due to the nuclear wave function

$$S(t) = \left(\frac{\sqrt{(2\pi)^3 2m}}{16\pi} \right)^2 \int \frac{dk_1 k_1}{E_1} \frac{dk_2 k_2}{E_2} \frac{\Theta(E_\Theta - E_1)}{p_\Theta} \frac{\Theta(E_\Theta - E_2)}{p_\Theta} \times \Theta \left(-1 < \frac{E_\Theta E_1 - a}{p_\Theta k_1} < 1 \right) \Theta \left(-1 < \frac{E_\Theta E_2 - a}{p_\Theta k_2} < 1 \right) \rho_D(k_1, k_2), \quad (10)$$

where $\rho_D(k_1, k_2)$ is the unpolarized deuteron density matrix, which can be expressed in terms of the S (its wave function is denoted by $u(k)$) and D (its wave function is denoted by $w(k)$) waves of the deuteron wave function

$$\rho_D(k_1, k_2) = u(k_1)u(k_2) + w(k_1)w(k_2) \left(\frac{3}{2} \frac{(\vec{k}_1 \cdot \vec{k}_2)^2}{k_1^2 k_2^2} - \frac{1}{2} \right). \quad (11)$$

We used the Paris nucleon-nucleon potential for the deuteron wave function [17].

Appendix B

In this appendix we give expressions for the interference and purely background cross sections. We also present explicit expressions for the double and triple differential cross sections plotted in Figs. 8 and 9.

The scattering amplitude for the background reaction in Fig. 7 reads

$$\mathcal{A}^{\text{BG}} = -\bar{u}(p_\Lambda) \hat{\Gamma}_\Lambda^p \frac{\hat{p}_D - \hat{k} + m}{(p_D - k)^2 - m^2 + i0} \bar{u}(p_s) \hat{\Gamma}_D, \quad (12)$$

which, after the non-relativistic reduction of $\hat{\Gamma}_D$ (see Eq. (7)), becomes

$$\mathcal{A}^{\text{BG}} = -\sqrt{(2\pi)^3 2m} \bar{u}(p_\Lambda) \hat{\Gamma}_\Lambda^p u(p_D - p_s) \psi_D(p_s). \quad (13)$$

This amplitude interferes with the signal amplitude (see also Eq. (6))

$$\begin{aligned} \mathcal{A}^{\text{Signal}} = & -i \int \frac{d^4 k}{(2\pi)^4} \bar{u}(p_s) \hat{\Gamma}_\Theta \frac{\hat{p}_\Theta + M_\Theta}{p_\Theta^2 - M_\Theta^2 + i\Gamma^{\text{tot}} M_\Theta} \hat{\Gamma}_\Theta \frac{\hat{k} + m}{k^2 - m^2 + i0} \frac{1}{(p_\Theta - k)^2 - m_K^2 + i0} \\ & \times \bar{u}(p_\Lambda) \hat{\Gamma}_\Lambda^{p+n} \frac{\hat{p}_D - \hat{k} + m}{(p_D - k)^2 - m^2 + i0} \hat{\Gamma}_D. \end{aligned} \quad (14)$$

Keeping only the imaginary part of the loop integral (which is a dominant contribution) and performing the non-relativistic reduction (see Eq. (7)), the amplitude in Eq. (13) becomes

$$\begin{aligned} \mathcal{A}^{\text{Signal}} = & -i \left(\frac{\sqrt{(2\pi)^3 2m}}{16\pi} \right) \frac{1}{16\pi} \int \frac{dk k}{E} \frac{\Theta(E_\Theta - E)}{p_\Theta} \Theta \left(-1 < \frac{E_\Theta E - a}{p_\Theta k} < 1 \right) \\ & \times \bar{u}(p_s) \hat{\Gamma}_\Theta \frac{\hat{p}_\Theta + M_\Theta}{p_\Theta^2 - M_\Theta^2 + i\Gamma^{\text{tot}} M_\Theta} \hat{\Gamma}_\Theta u(k) \bar{u}(p_\Lambda) \hat{\Gamma}_\Lambda^{p+n} u(p_D - k) \psi_D(k). \end{aligned} \quad (15)$$

Near the resonance $p_\Theta^2 - M_\Theta^2 \ll \Gamma^{\text{tot}} M_\Theta$ and, hence, the signal amplitude is predominantly real. Therefore, $\mathcal{A}^{\text{Signal}}$ interferes with \mathcal{A}^{BG} and this interference is constructive (both amplitudes have a negative sign in front of them).

The interference cross section is obtained using Eqs. (13) and (15) and can be cast in the form of Eq. (1)

$$\frac{d\sigma^I}{dt} = 2\pi \Gamma^{\text{tot}} \frac{M_\Theta^3}{\sqrt{(M_\Theta^2 - m^2 - m_K^2)^2 - 4m^2 m_K^2}} \frac{d\sigma_{\text{elem}}^I}{dt} S(t), \quad (16)$$

where

$$\frac{d\sigma_{\text{elem}}^I}{dt} = \frac{1}{64\pi(E_\gamma m)^2} ((\mathcal{A}^p + \mathcal{A}^n)(\mathcal{A}^p)^* + (\mathcal{A}^p + \mathcal{A}^n)^* \mathcal{A}^p). \quad (17)$$

While the signal and interference cross sections have a similar appearance, the double differential signal and interference cross sections have distinctly different dependences on the momentum of the neutron in the final state p_s . When we take into account the decay of Θ^+ into the nK^+ final state, Eq. (1) should be multiplied by the branching ratio of the $\Theta^+ \rightarrow nK^+$ decay (which equals 1/2) and by the nK^+ phase space. The $\gamma + D \rightarrow \Lambda(\Sigma) + \Theta^+ \rightarrow \Lambda(\Sigma) + n + K^+$ double differential cross section then reads

$$\begin{aligned} \frac{d^2\sigma}{dt dp_s} = & 2\pi \Gamma^{\text{tot}} \frac{M_\Theta^3}{\sqrt{(M_\Theta^2 - m^2 - m_K^2)^2 - 4m^2 m_K^2}} \frac{d\sigma^{p+n}}{dt} S(t) \\ & \times \frac{1}{2} \frac{M_\Theta}{2p_\Theta k^*} \frac{p_s}{E_s} \Theta \left(-1 < \frac{m_K^2 + p_\Theta^2 + p_s^2 - (E_\Theta - E_s)^2}{2p_\Theta p_s} < 1 \right), \end{aligned} \quad (18)$$

where k^* is the spectator momentum in the Θ^+ rest frame.

The p_s dependence of the interference cross section is determined by the deuteron wave function and the double differential cross section reads

$$\frac{d^2\sigma^I}{dt dp_s} = 2\pi\Gamma^{tot} \frac{M_\Theta^3}{\sqrt{(M_\Theta^2 - m^2 - m_K^2)^2 - 4m^2m_K^2}} \frac{d\sigma_{\text{elem}}^I}{dt} \frac{dS(t, p_s)}{dp_s}, \quad (19)$$

where (see also Eq. (10))

$$\frac{dS(t, p_s)}{dp_s} = \left(\frac{\sqrt{(2\pi)^3 2m}}{16\pi} \right)^2 \int \frac{dkk}{E_k} \frac{p_s}{E_s} \frac{\Theta(E_\Theta - E_k)}{p_\Theta} \frac{\Theta(E_\Theta - E_s)}{p_\Theta} \times \Theta \left(-1 < \frac{E_\Theta E_k - a}{p_\Theta k} < 1 \right) \Theta \left(-1 < \frac{E_\Theta E_s - a}{p_\Theta p_s} < 1 \right) \rho_D(k, p_s). \quad (20)$$

The sum of Eqs. (18) and (20) is presented in Fig. 8 by solid curves. The interference cross section of Eqs. (20) is presented by dash-dotted curves in Fig. 8.

The double differential cross section of the purely background process based on the amplitude of Eq. (13) takes the form

$$\frac{d^2\sigma^{\text{BG}}}{dt dp_s} = \pi m m_D \frac{p_s}{E_s} |\psi_D(p_s)|^2 \frac{d\sigma^p}{dt} \int_{E_\Lambda^{\text{min}}}^{E_\Lambda^{\text{max}}} \frac{dE_\Lambda}{2|p_\gamma - p_\Lambda|} \Theta \left(-1 < \frac{m_K^2 + |p_\gamma - p_\Lambda|^2 + p_s^2 - b^2}{2p_s|p_\gamma - p_\Lambda|} < 1 \right), \quad (21)$$

where p_Λ is the momentum of Λ in the deuteron rest frame; $b = E_\gamma + m_D - E_s - E_\Lambda$; $d\sigma^p/dt$ is the cross section of the $\gamma + p \rightarrow \Lambda(\Sigma) + K^+$ reaction. The upper and lower limits of integration over E_Λ are determined by the condition on the $n - K^+$ invariant mass (see Eq. (4))

$$E_\Lambda^{\text{min,max}} = (t + m_D^2 + 2m_D E_\gamma - (M_\Theta \pm 0.010)^2) / (2m_D). \quad (22)$$

This cross section is given by dashed curves in Fig. 8.

If the experimental resolution in the invariant mass of the final K^+n system is at the level of a few MeV and statistics is high, one can also study the signal, interference and background cross sections as functions of the invariant mass $M^2 = (p_s + p_K)^2$. The resulting expressions read

$$\begin{aligned} \frac{d^3\sigma}{dt dp_s dM^2} &= \frac{d\sigma}{dt dp_s} \frac{\Gamma^{tot} M_\Theta}{\pi} \frac{1}{(M^2 - M_\Theta^2)^2 + (\Gamma^{tot} M_\Theta)^2}, \\ \frac{d^3\sigma^I}{dt dp_s dM^2} &= \frac{d\sigma^I}{dt dp_s} \frac{\Gamma^{tot} M_\Theta}{\pi} \frac{1}{(M^2 - M_\Theta^2)^2 + (\Gamma^{tot} M_\Theta)^2} + \dots, \\ \frac{d^3\sigma^{\text{BG}}}{dt dp_s dM^2} &= \pi m \frac{p_s}{E_s} |\psi_D(p_s)|^2 \frac{d\sigma^p}{dt} \frac{1}{4|p_\gamma - p_\Lambda|} \Theta \left(-1 < \frac{m_K^2 + |p_\gamma - p_\Lambda|^2 + p_s^2 - b^2}{2p_s|p_\gamma - p_\Lambda|} < 1 \right) \end{aligned} \quad (23)$$

In the second line, the dots denote a correction which introduces a small deviation of the interference cross section from the pure Breit-Wigner form. The cross sections of Eq. (23) are presented in Fig. 9.

- [1] D. Diakonov, V. Petrov and M. Polyakov, Z. Phys. A **359** (1997) 305.
- [2] SPRING8 Collab., T. Nakano *et al.*, Phys. Rev. Lett. **91** (2003) 012002.
- [3] DIANA Collab., V.V. Barmin *et al.*, Phys. Atom. Nucl. **66** (2003) 1715 [Yad. Fiz. **66** (2003) 1763]; preprint hep-ex/0304040.
- [4] CLAS Collab., S. Stepanyan *et al.*, Phys. Rev. Lett. **91** (2003) 252001 [hep-ex/0307018].
- [5] CLAS Collab. V. Kubarovsky *et al.*, Phys. Rev. Lett. **92** (2004) 032001; Erratum-ibid. **92** (2004) 049902 [hep-ex/0311046].
- [6] A.E. Asratyan, A.G. Dolgolenko and M.A. Kubantsev, preprint hep-ex/0309042, submitted to Phys. At. Nucl. (Yad. Fiz.).
- [7] SAPHIR Collab., J. Barth *et al.*, Phys. Lett. B **572** (2003) 127 [hep-ex/0307083].
- [8] HERMES Collab., A. Airapetian *et al.*, Phys. Lett. B **585** (2004) 213 [hep-ex/0312044].
- [9] SVD Collab., A. Aleev *et al.*, preprint hep-ex/0401024, submitted to Yad. Fiz.
- [10] COSY-TOF Collab., M. Abdel-Bary *et al.*, preprint hep-ex/0403011.
- [11] ZEUS Collab., S. Chekanov *et al.*, preprint hep-ex/0403051.
- [12] GRAAL Collab., C. Schaerf, talk at the Pentaquark 2003 workshop, Jefferson Lab, Newport News, Virginia, November 2003.
- [13] MAID 2000 data base, <http://www.kph.uni-mainz.de>. Kaon-MAID model is based on F.X. Lee, T. Mart, C. Bennhold, H. Haberzettl, L.E. Wright, Nucl. Phys. A **695** (2001) 237 [nucl-th/9907119] and T. Mart and C. Bennhold, Phys. Rev. C **61** (2000) 012201 [nucl-th/9906096].
- [14] SAPHIR Collab., M.Q. Tran *et al.*, Phys. Lett. B **445** (1998) 20.
- [15] C. Bennhold *et al.*, Nucl. Phys. A **639** (1998) 209c.
- [16] SAPHIR Collab., K.-H. Glander *et al.*, Eur. Phys. J. A **19** (2004) 251 [nucl-ex/0308025].
- [17] M. Lacombe *et al.*, Phys. Lett. B **101** (1981) 139.
- [18] R.A. Arndt, I.I. Strakovsky and R.L. Workman, Phys. Rev. C **68** (2003) 042201(R).
- [19] R.N. Cahn and G.H. Trilling, Phys. Rev. D **69** (2004) 011501(R).

- [20] S. Capstick, P.R. Page and W. Roberts, Phys. Lett. B **570** (2003) 185 [hep-ph/03070].
- [21] P.R. Page, preprint hep-ph/0310200.
- [22] M.P. Rekalo and E. Tomasi-Gustafsson, preprint hep-ph/0401050.